
# Transient Three-Dimensional Analysis of Nozzle Side Load in Regeneratively Cooled Engines AIAA 2005-3942

Ten-See Wang

ER43, Thermal and Combustion Analysis Branch

Propulsion Structure, Thermal, and Fluids Analysis Division

NASA – Marshall Space Flight Center

41st AIAA/ASME/SAE/ASEE Joint Propulsion Conference and Exhibit

Tucson, Arizona, July 10-13, 2005

# Acknowledgment


- MSFC FY03 CDDF entitled "Nozzle Side Load Technology"
- Werner Dahm, Dave Seymour, and Joe Ruf
- Y.-S. Chen of Engineering Sciences, Inc.
- James Beck of Boeing Rocketdyne

# Introduction


- Nozzle side loads are potentially detrimental to the integrity and life of almost all launch vehicles.
- The lack of a detailed prediction capability results in reduced life and increased weight for reusable nozzle systems.
- A clear understanding of the mechanisms that contribute to side loads during engine startup, shutdown, and steady-state operations must be established. A CFD based predictive tool must be developed to aid the understanding of side load physics and development of future reusable engines.

# Introduction Continued


- CFD transient nozzle side load studies
  - Wang on an axisymmetric SSME nozzle hot-firing, 1992
    - Equilibrium reacting flow, simulated startup & shutdown sequence
  - Chen, et al. on an axisymmetric cold flow J2S nozzle, 1994
    - Cold flow, impulse start
  - Yonezawa, et al. on 2-D LE-7A nozzle side load, 2002
    - Cold flow, linear ramp rate in pressure
    - 32.5% Ar + 67.5% N2 @ $\gamma = 1.5$
  - Yonezawa, et al. on 3-D side loads for LE-7, LE-7A, and CTP50-R5-L nozzles, 2002
    - Frozen flow (25% $H_2$ + 75% $H_2O$), linear ramp rate in pressure & temperature for LE-7 and LE-7 A
    - Cold $N_2$ and linear ramp rate for CTP50-R5-L
  - Wang on 2-D and axisymmetric SSME nozzles, 2004
    - Fully chemical reacting flow with simulated engine start-up sequence
    - Coanda effect, afterburning wave, FSS to RSS and vice versa, and lip lambda shock oscillation.
    - Factors affect side load physics: ramp rate and reaction

# Objectives


- Identify the 3-D Block-I SSME start-up side load physics and compute the associated aerodynamic side load using an anchored computational methodology
- Study the effect of (regenerative) wall cooling on side load physics

# Governing Equations


$$\frac{\partial \rho}{\partial t}+\frac{\partial}{\partial x_j}\left(\rho u_j\right)=0$$

$$\frac{\partial \rho \alpha_i}{\partial t}+\frac{\partial}{\partial x_j}\left(\rho u_j \alpha_j\right)=\frac{\partial}{\partial x_j}\left[\left(\rho D+\frac{\mu_t}{\sigma_\alpha}\right)\right]+\omega_i$$

$$\frac{\partial \rho u_i}{\partial t}+\frac{\partial}{\partial x_j}\left(\rho u_j u_i\right)=-\frac{\partial p}{\partial x_i}+\frac{\partial \tau_{ij}}{\partial x_j}$$

$$\frac{\partial \rho H}{\partial t}+\frac{\partial}{\partial x_j}\left(\rho u_j H\right)=\frac{\partial p}{\partial t}+Q_r+\frac{\partial}{\partial x_j}\left[\left(\frac{K}{C_p}+\frac{\mu_t}{\sigma_H}\right)\nabla H\right]+\frac{\partial}{\partial x_j}\left\{\left[\left(\mu+\mu_t\right)-\left(\frac{K}{C_p}+\frac{\mu_t}{\sigma_H}\right)\right]\nabla\left(\frac{V^2}{2}\right)\right\}+\theta$$

$$\frac{\partial \rho k}{\partial t}+\frac{\partial}{\partial x_j}\left(\rho u_j k\right)=\frac{\partial}{\partial x_j}\left[\left(\mu+\frac{\mu_t}{\sigma_k}\right)\frac{\partial k}{\partial x_j}\right]+\rho\left(\Pi-\varepsilon\right)$$

$$\frac{\partial \rho \varepsilon}{\partial t}+\frac{\partial}{\partial x_j}\left(\rho u_j \varepsilon\right)=\frac{\partial}{\partial x_j}\left[\left(\mu+\frac{\mu_t}{\sigma_\varepsilon}\right)\frac{\partial \varepsilon}{\partial x_j}\right]+\rho\frac{\varepsilon}{k}\left(C_1\Pi-C_2\varepsilon+C_3\frac{\Pi^2}{\varepsilon}\right)$$

# Simulated Start-Up Inlet Conditions

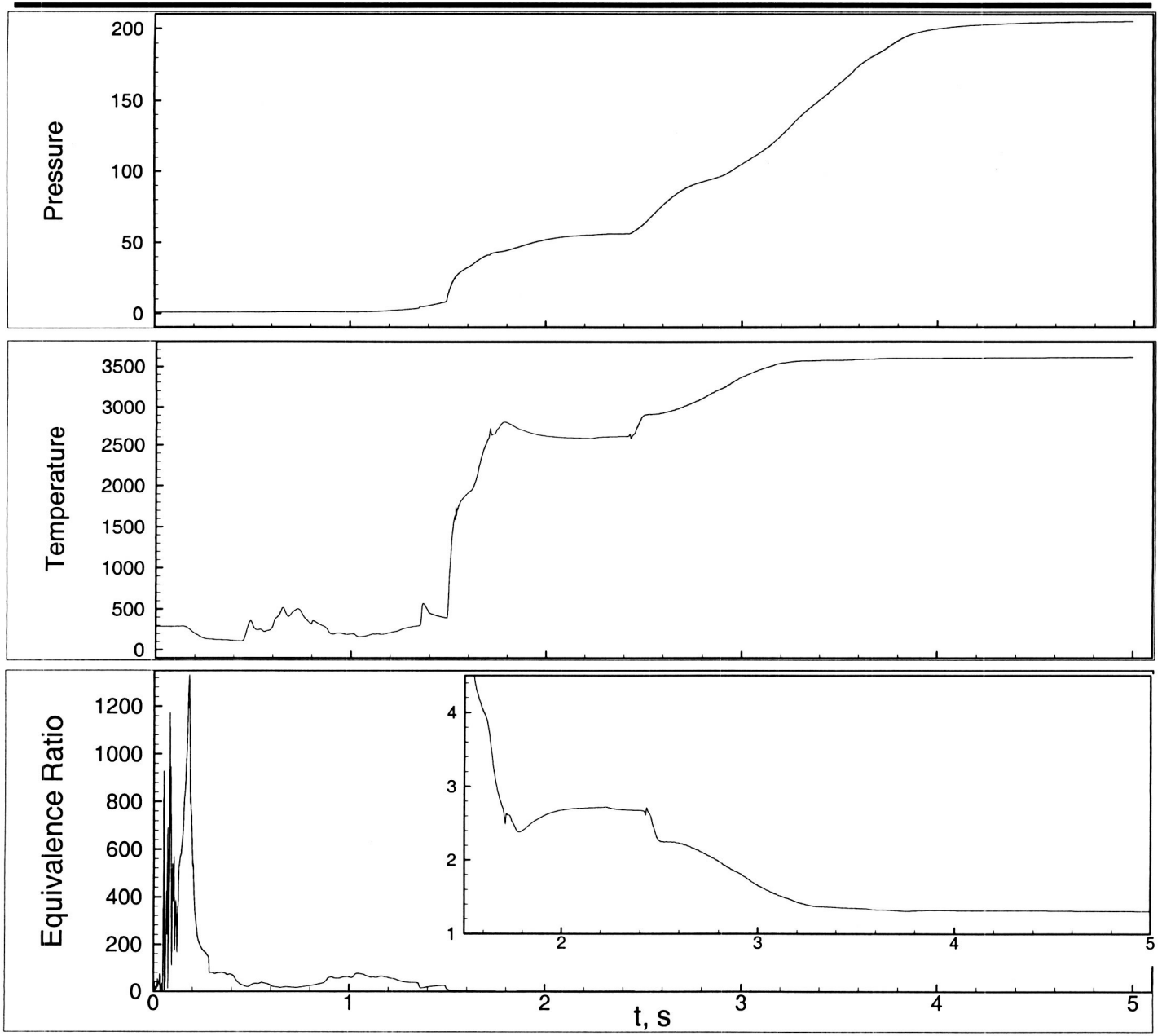

# Computational Grid


| Grid | # points | # cells | # structured cells | # unstructured cells |
|---|---|---|---|---|
| 3d6 | 1,286,934 | 1,275,120 | 1,101,600 | 173,520 |

# Computational Grid 3d6

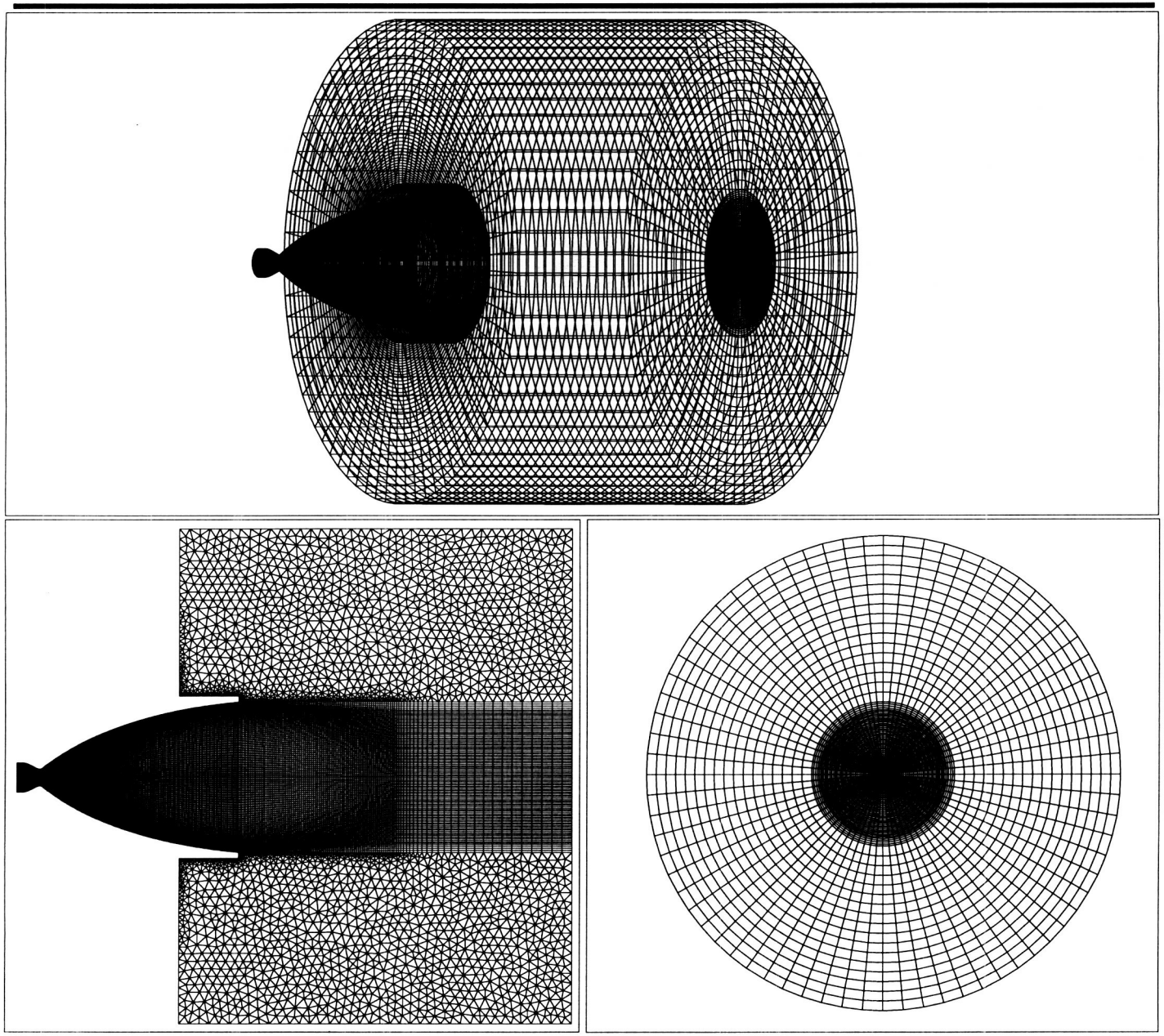

# Run Matrix

| geometry | chemistry | wall B.C. | ramp time |
|---|---|---|---|
| 3-D | finite-rate | adiabatic | 5 s |
| 3-D | finite-rate | cooled | 5 s |

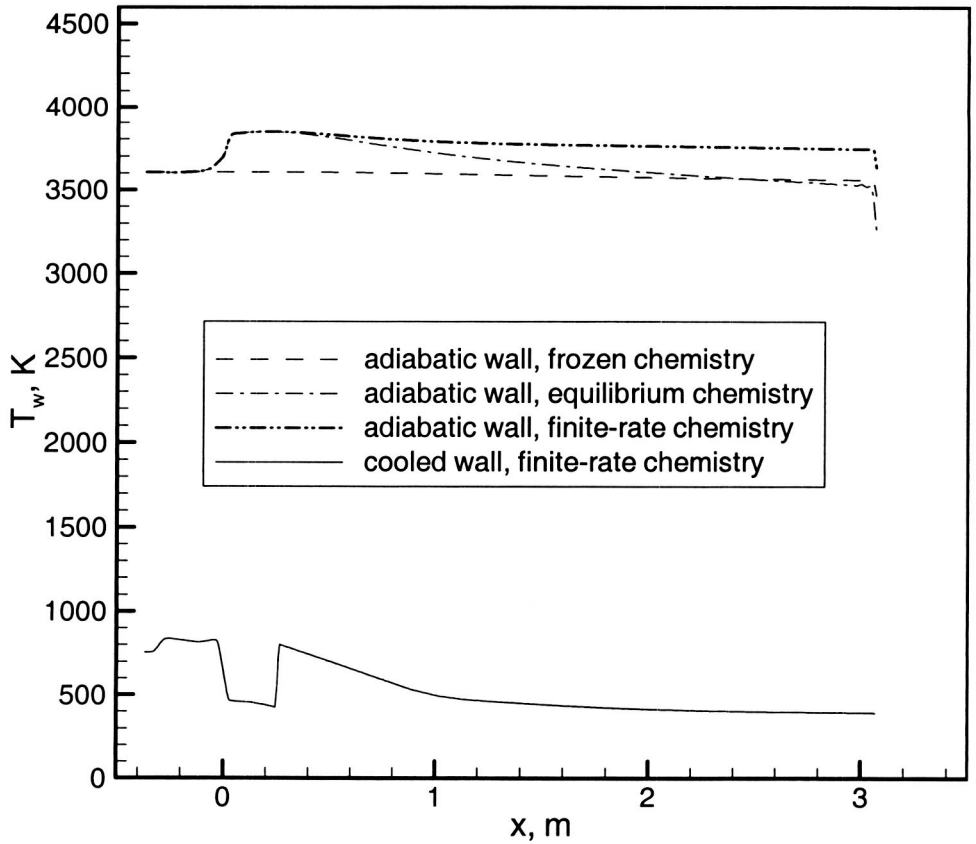

## Effect of cooled wall on flow separation


- In 1973, Nave & Coffey noted that colder walls tend to retard separation by observing flow separation during J-2S engine firing.
- In 1988, Chang, Krozon, and Merkle did steady CFD analyses on axisymmetric conical and contoured nozzles and found that cold wall B.C. results in a much thinner boundary layer than was computed for the hot-wall conditions. This thinner, cold wall boundary layer is also less susceptible to separation than were the hot-wall results.
- In 1994, Shimura, Asaka, and Lee did steady CFD analyses on a 2-D planar conical nozzle and reached similar conclusion as that of Chang, Krozen, and Merkle.

# Computed y-plane temperature contours of the cooled nozzle showing combustion wave

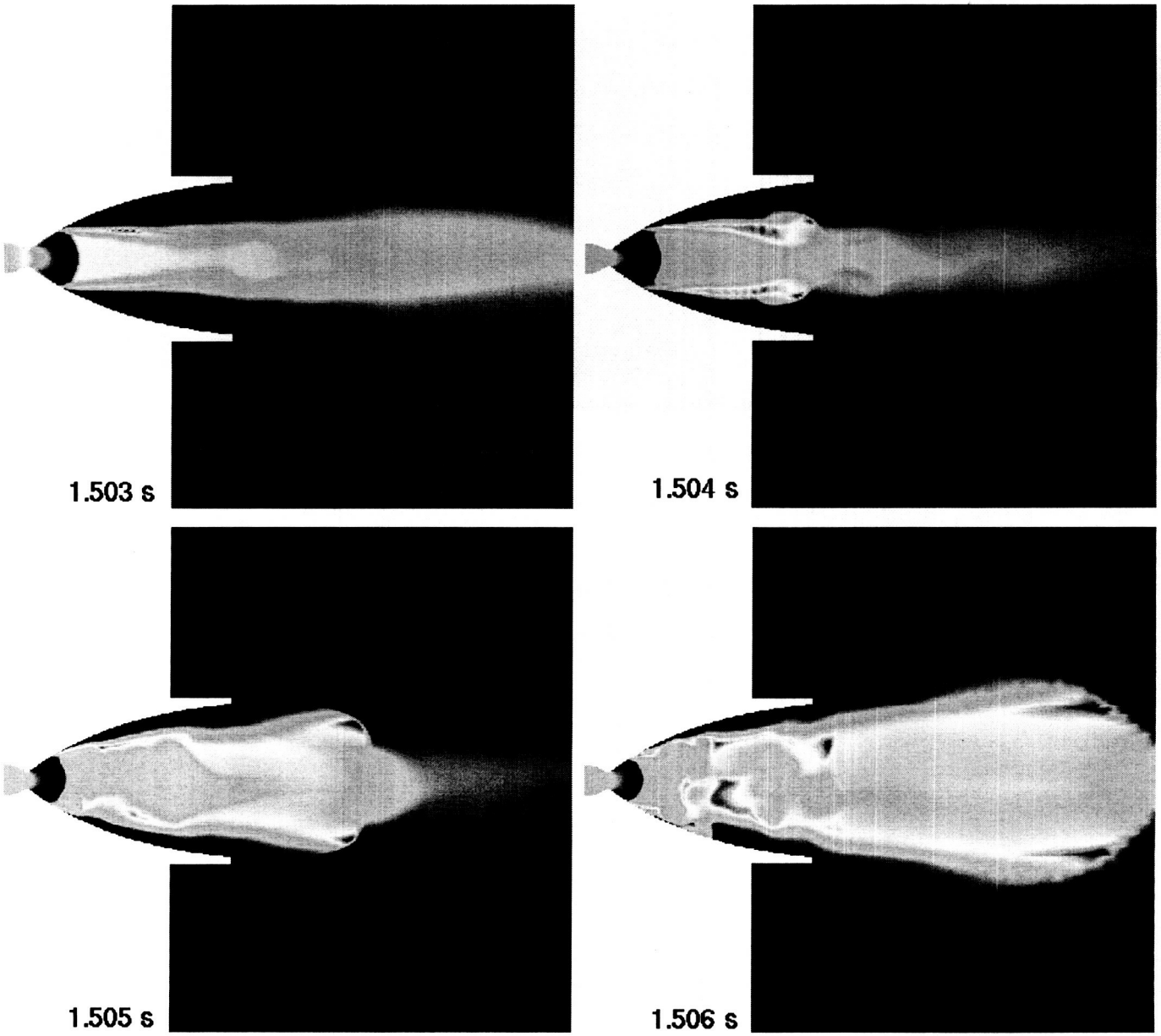

# Computed y-plane pressure contours of the cooled nozzle showing combustion wave

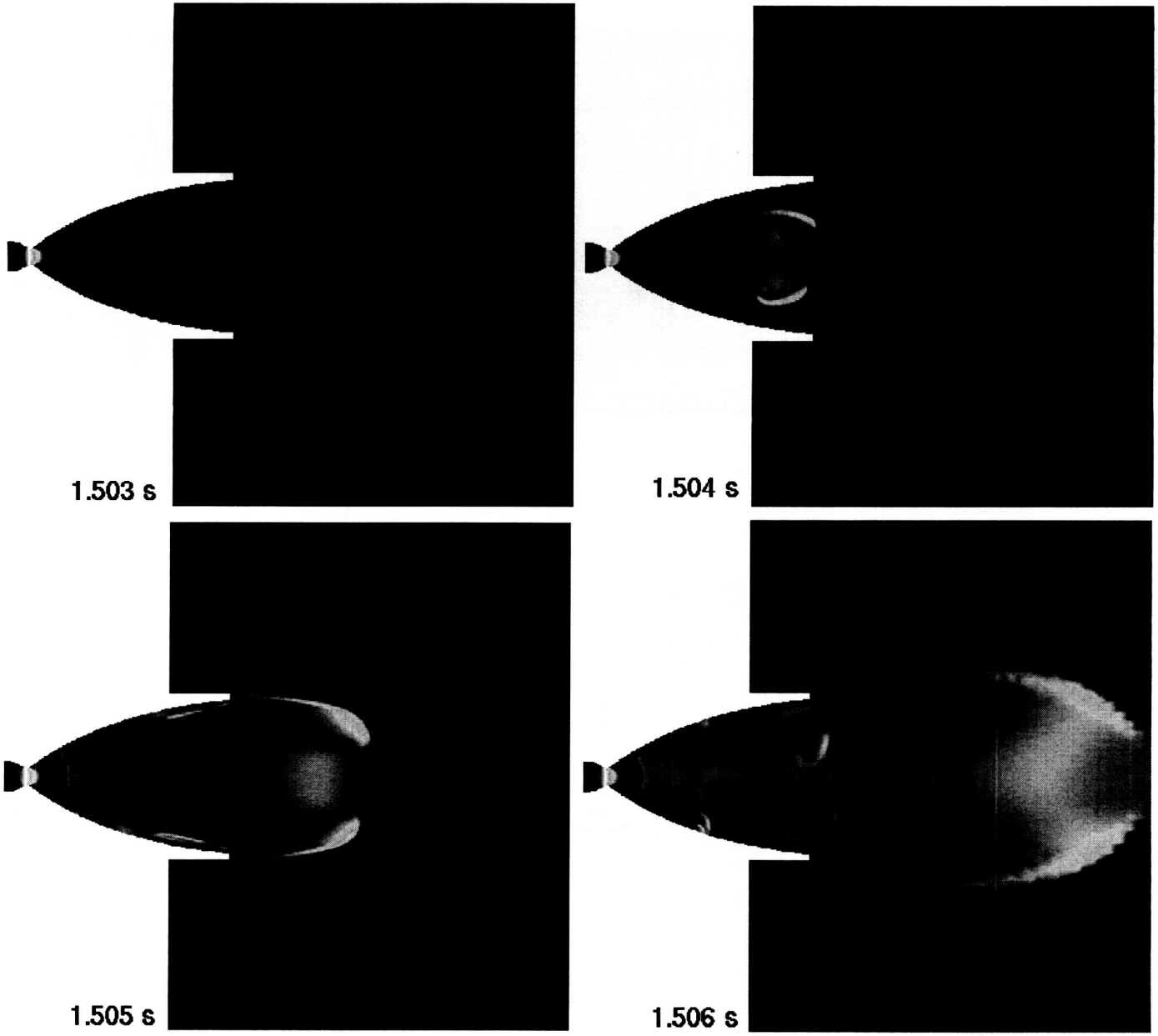

# Computed z-plane Mach number contours of the cooled nozzle showing FSS-to-RSS transition

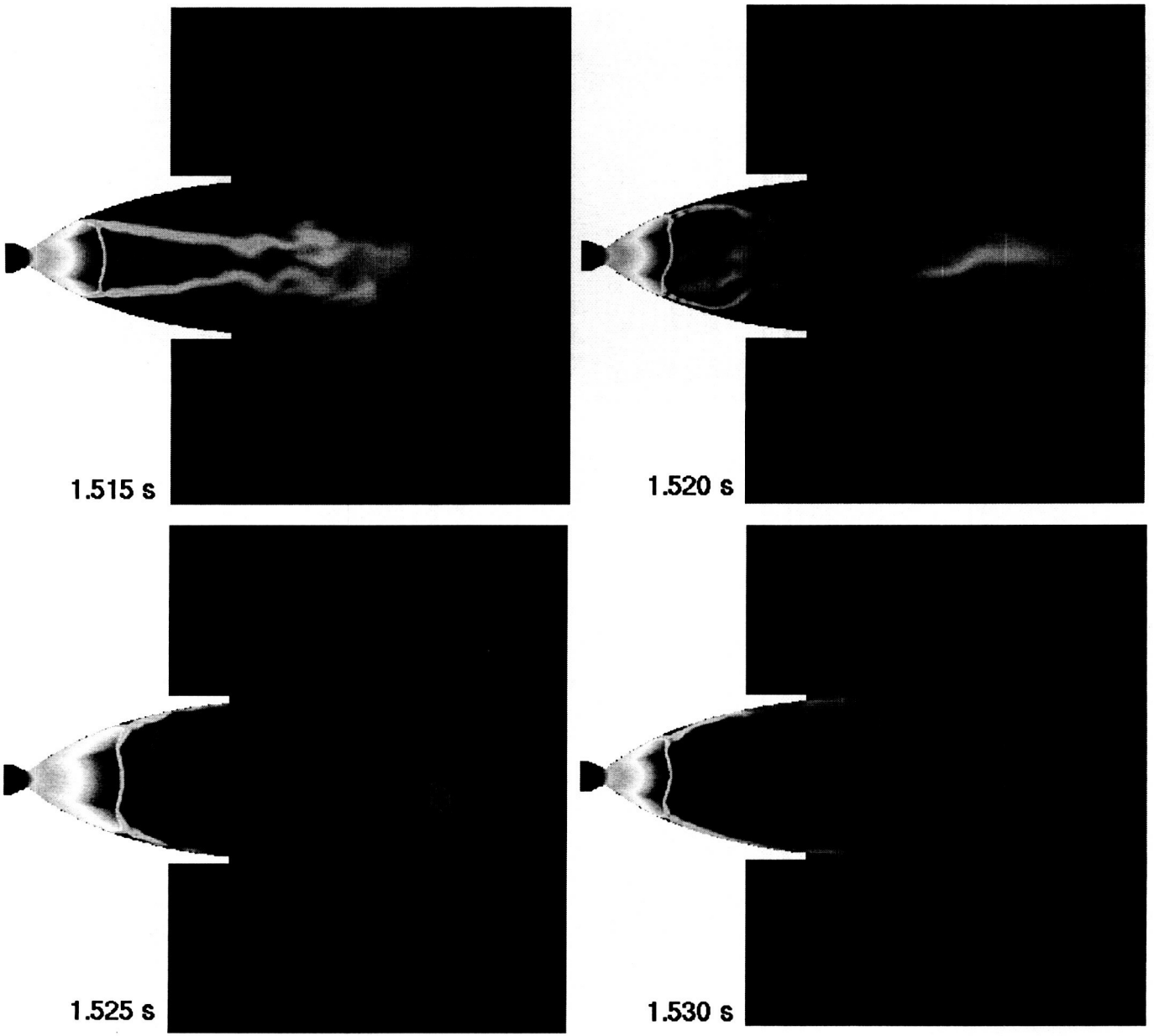

# Computed side forces for the adiabatic nozzle from 0 ~ 2 s

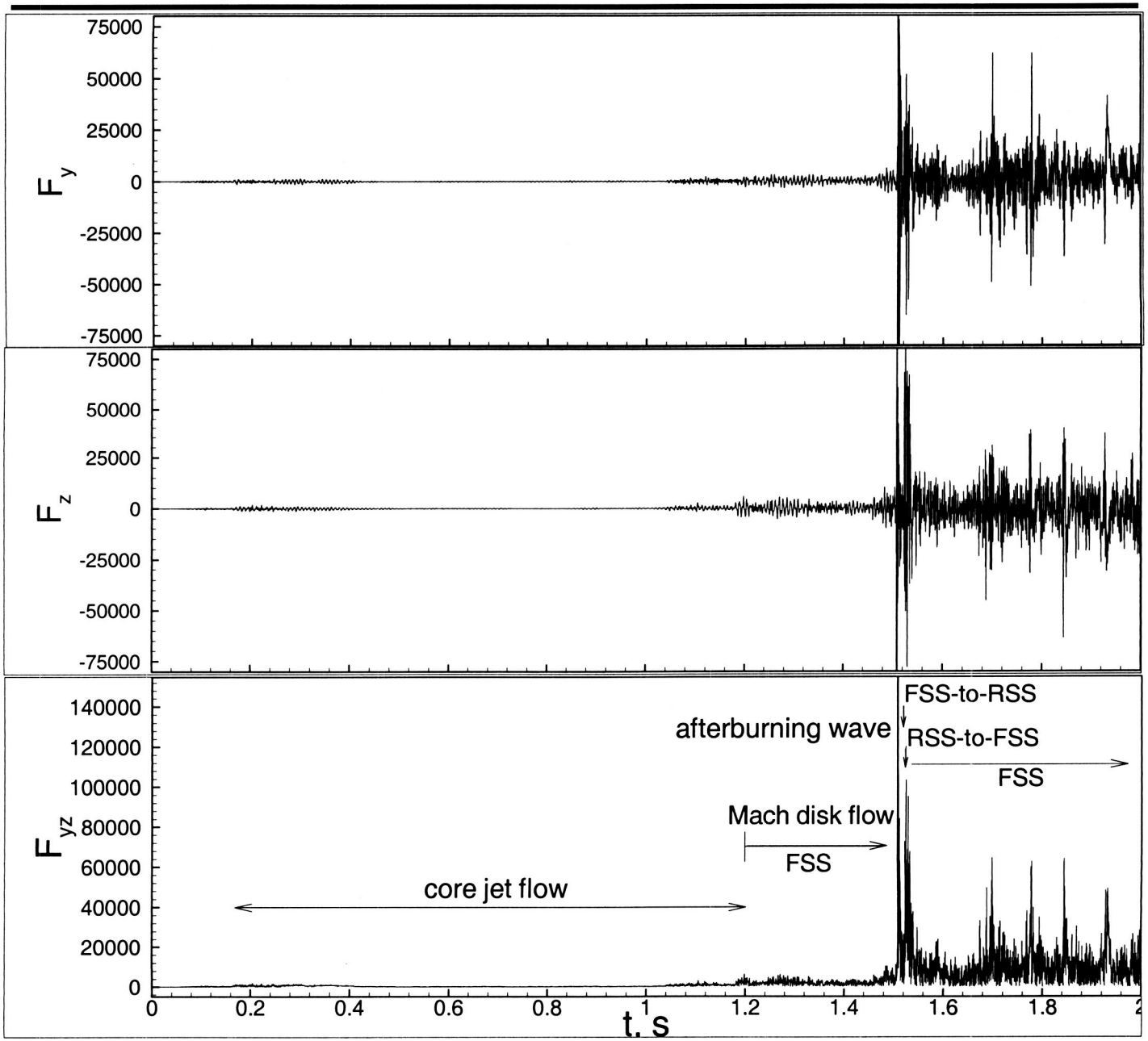

# Computed side forces for the cooled nozzle from 0 ~ 2 s

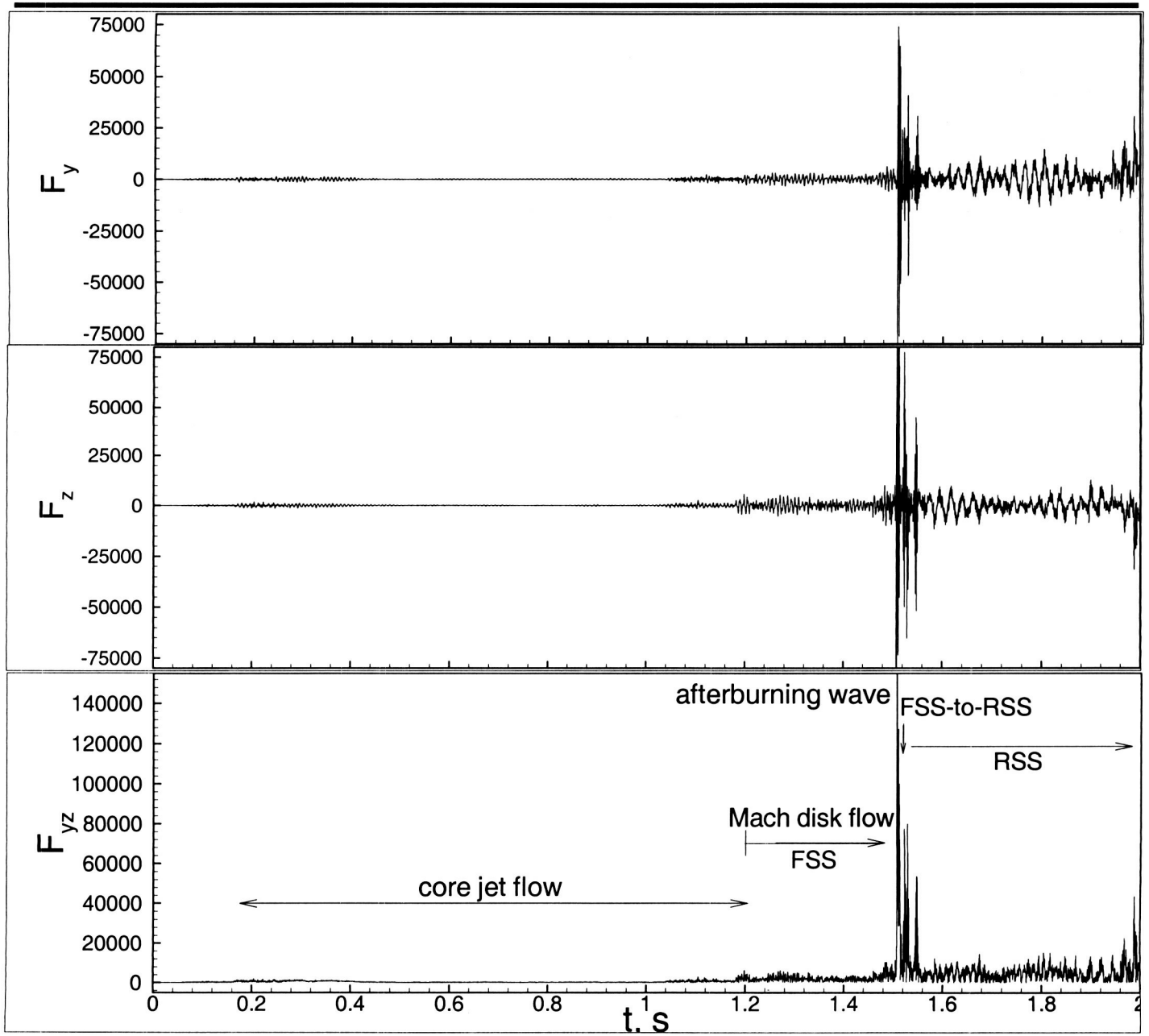

# Computed scalar contours for the adiabatic nozzle at 2.625 s

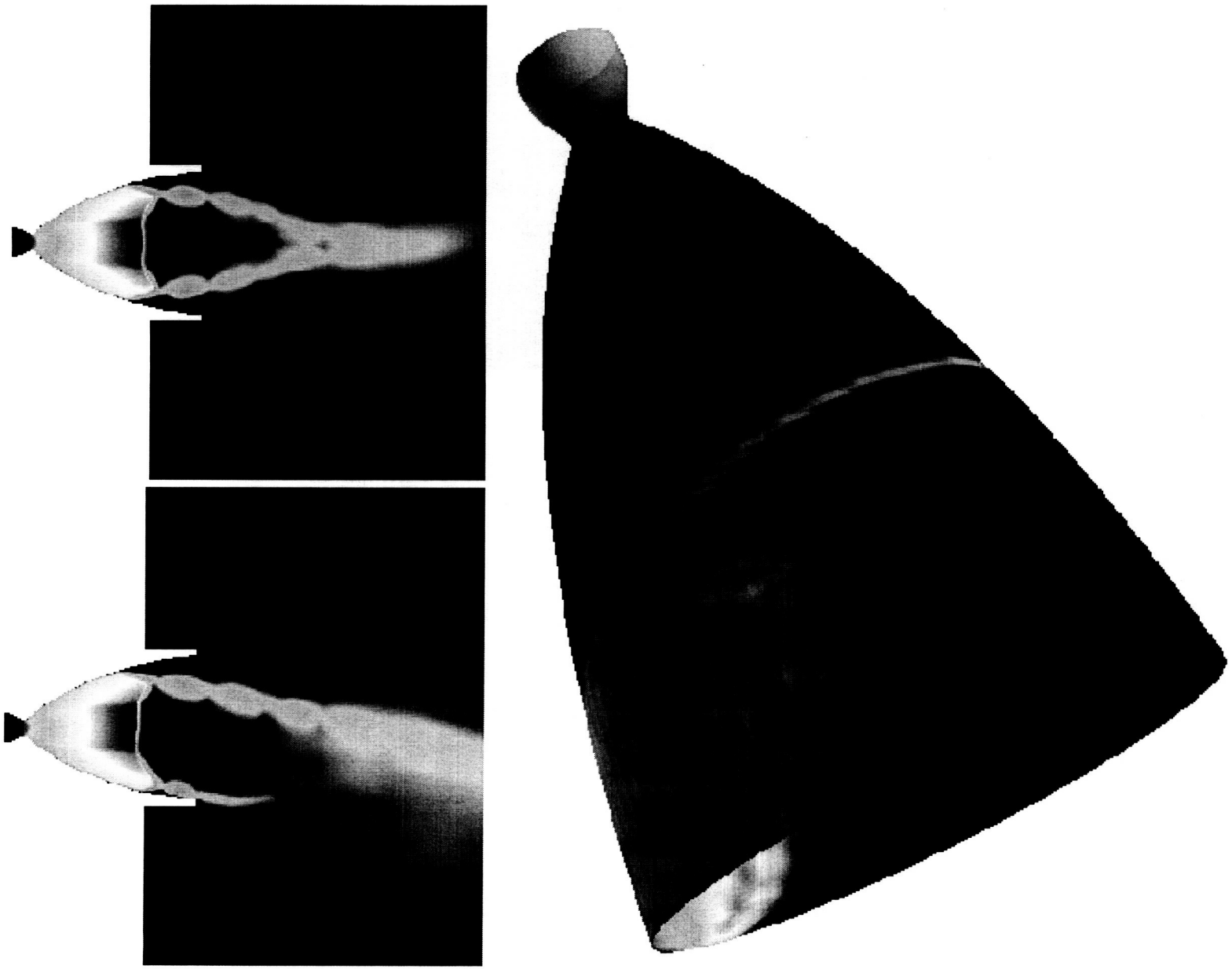

# Computed exhausting and receding wall OH contours for the adiabatic nozzle

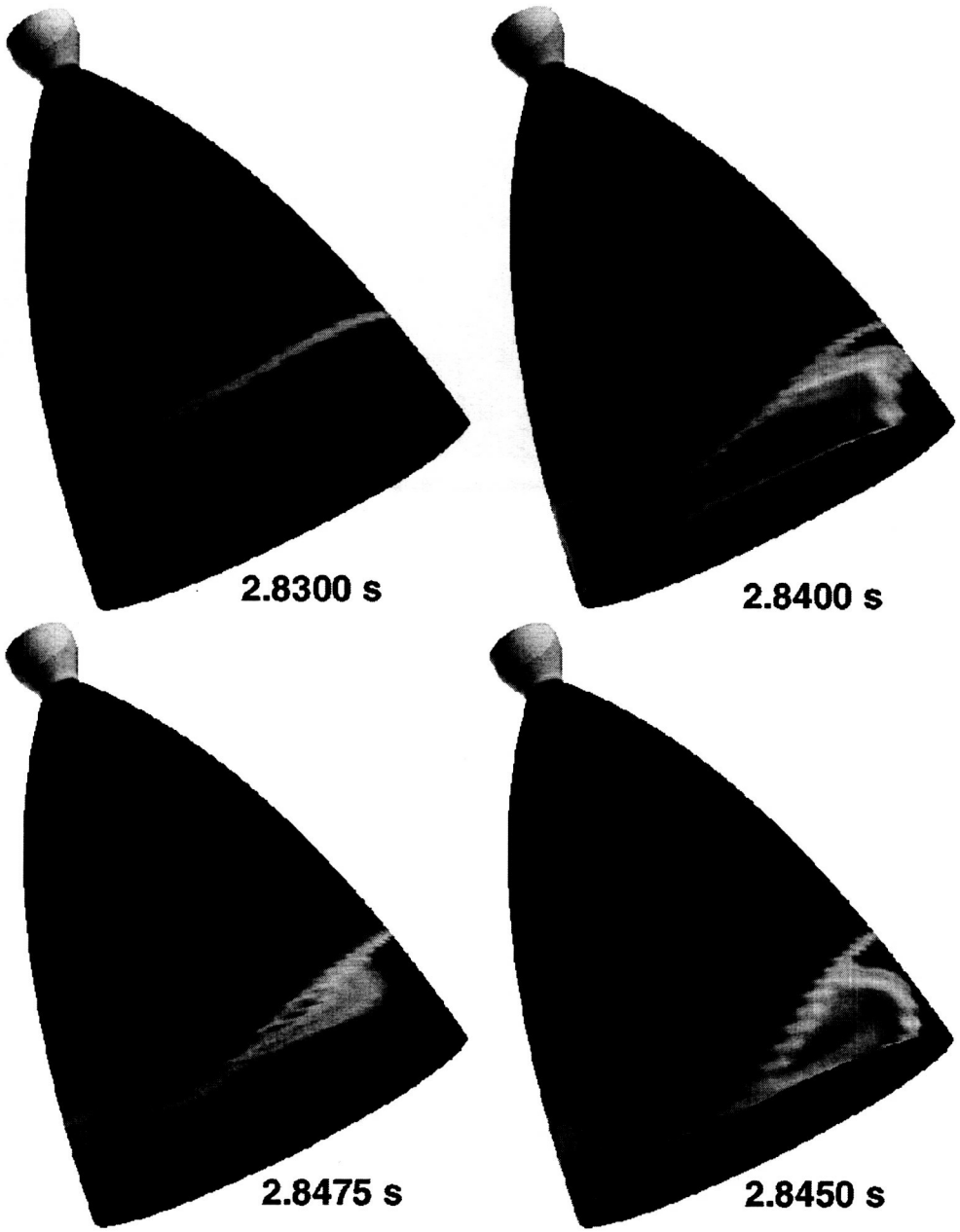

# Computed side force loci for the adiabatic nozzle

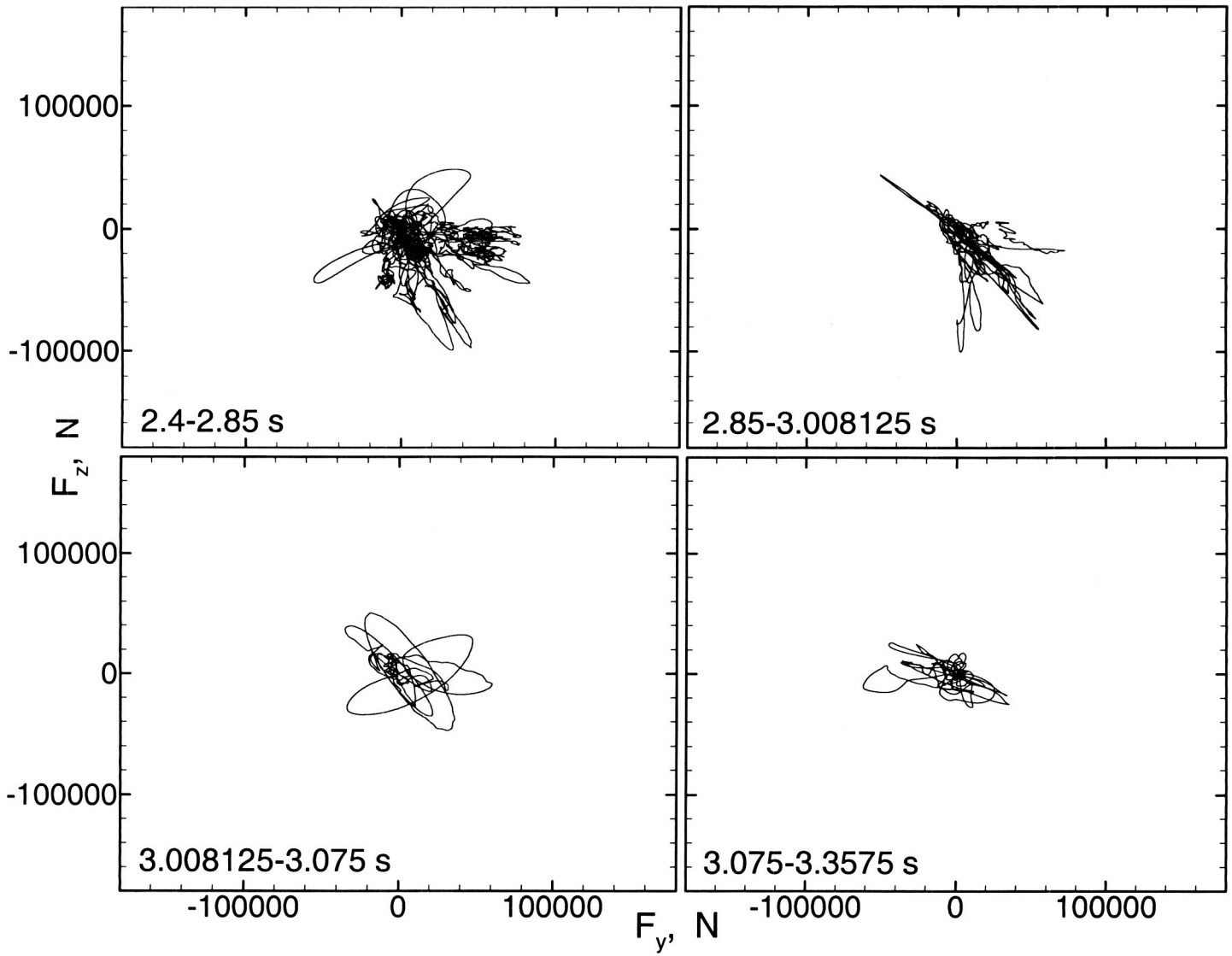

# Computed scalar contours for the cooled nozzle at 2.580 s

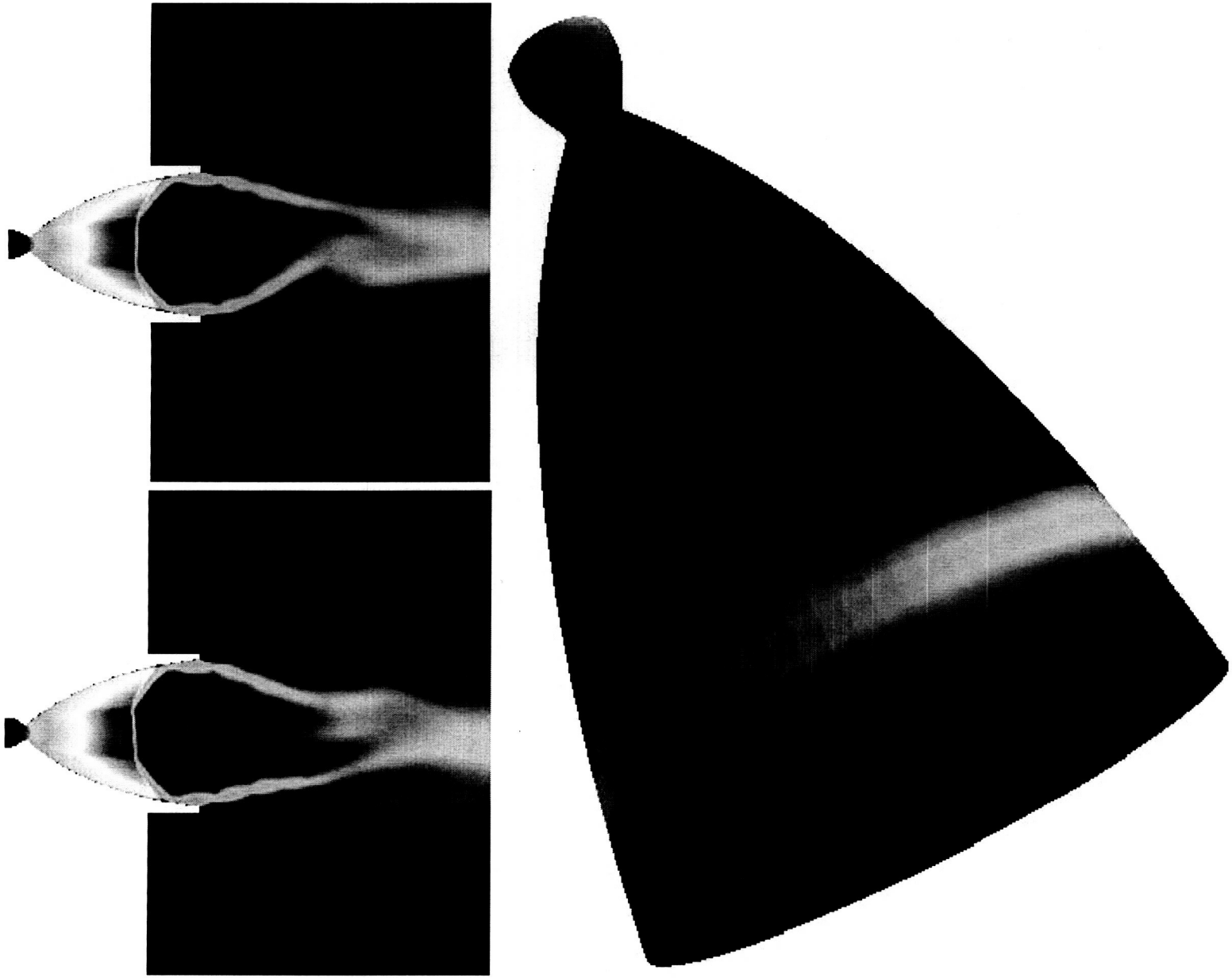

# Computed exhausting and receding wall OH contours for the cooled nozzle

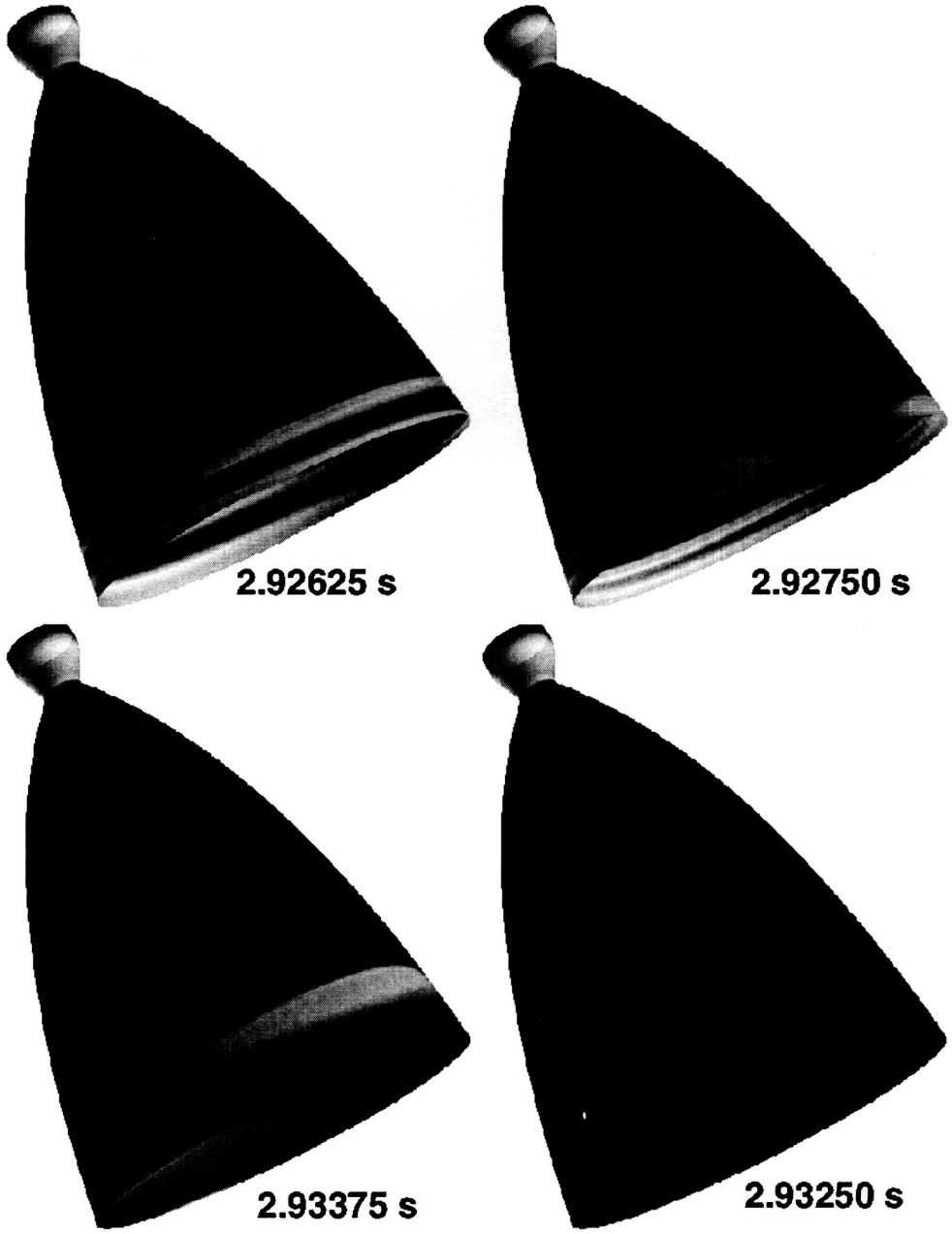

# Computed tangential force loci for the cooled nozzle

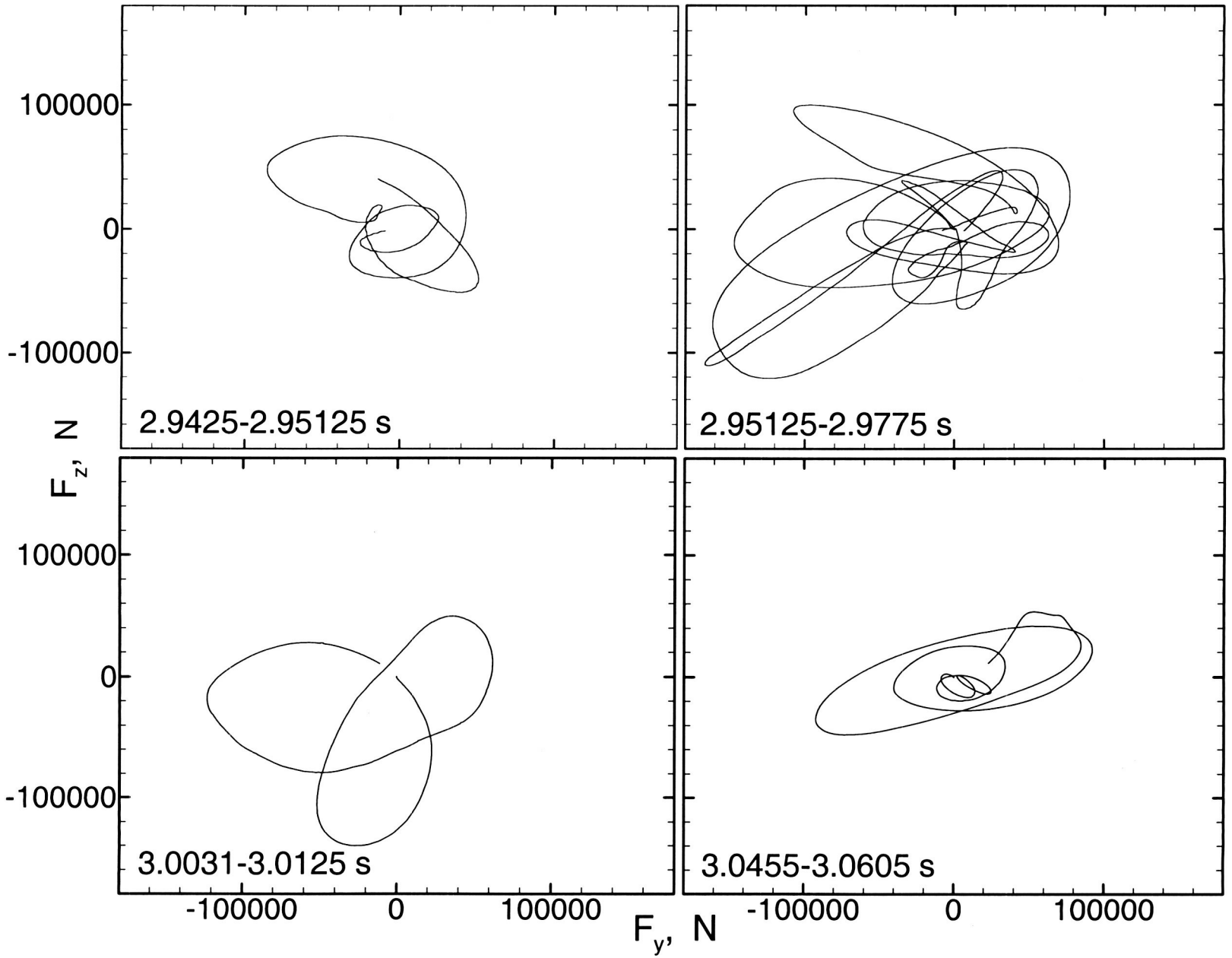

# Computed side forces for the adiabatic nozzle from 2 ~ 4 s

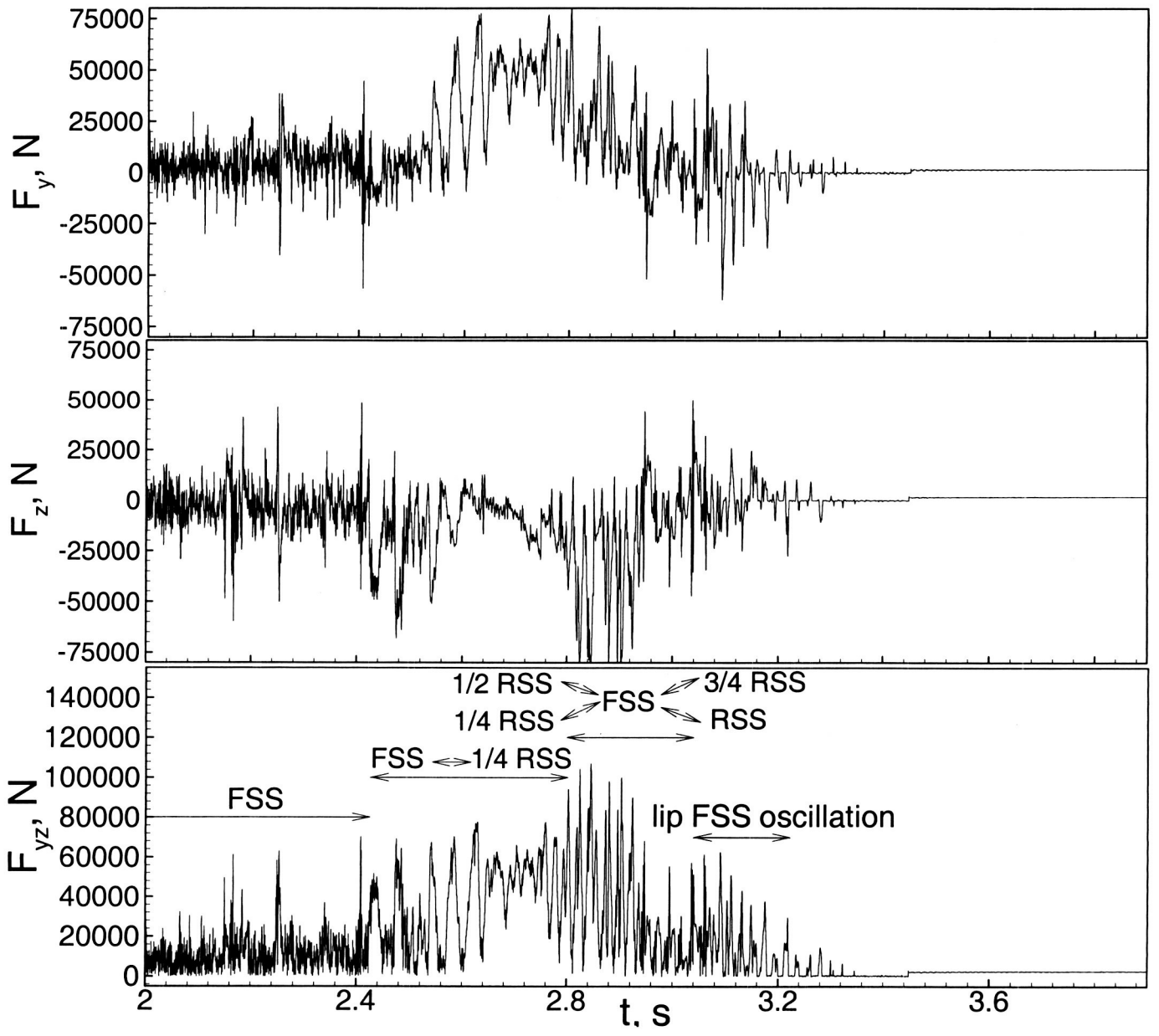

# Computed side forces for the cooled nozzle from 2 ~ 4 s

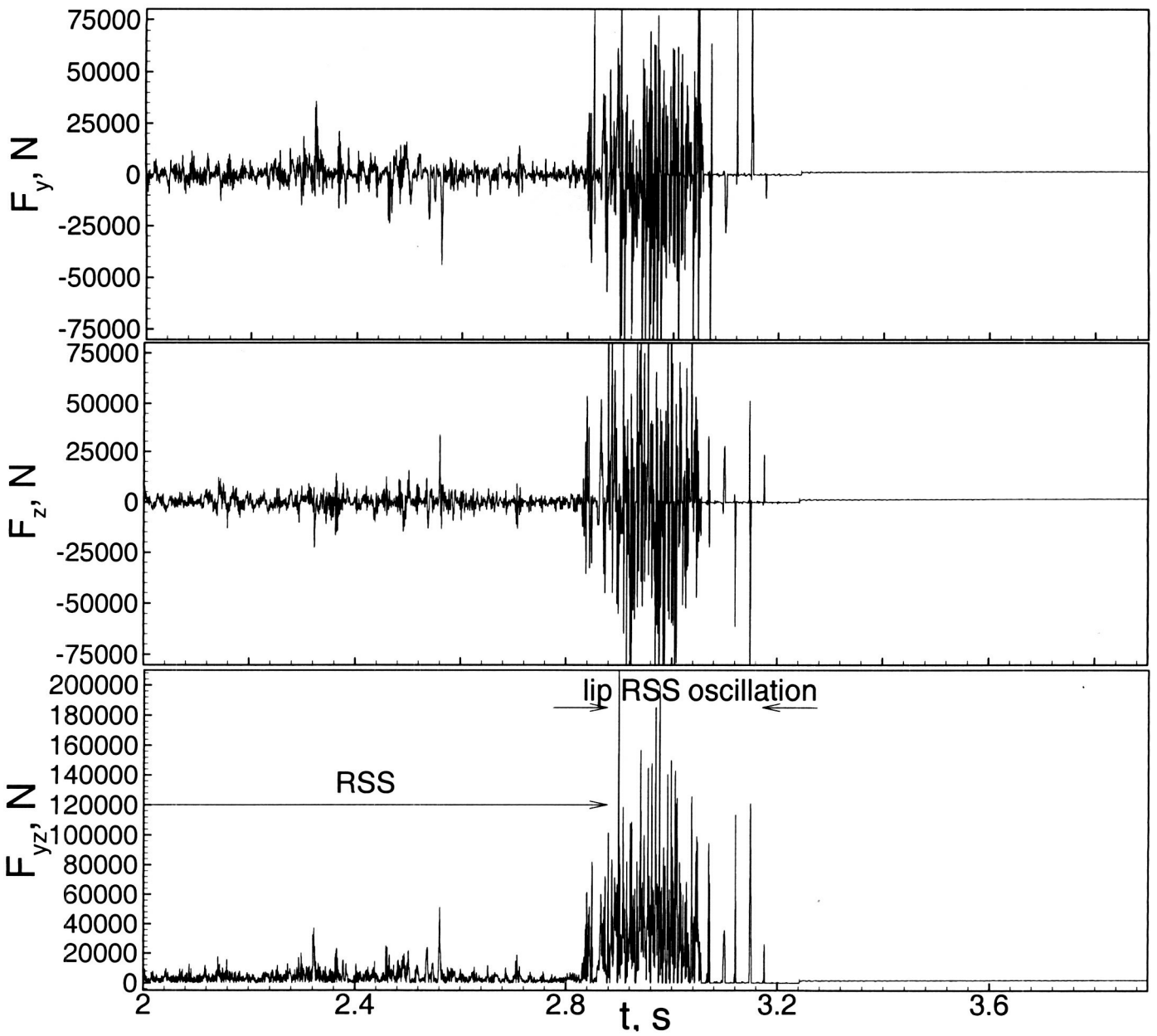

# Computed near lip wall pressure, shear stress, and heat flux histories for the cooled nozzle

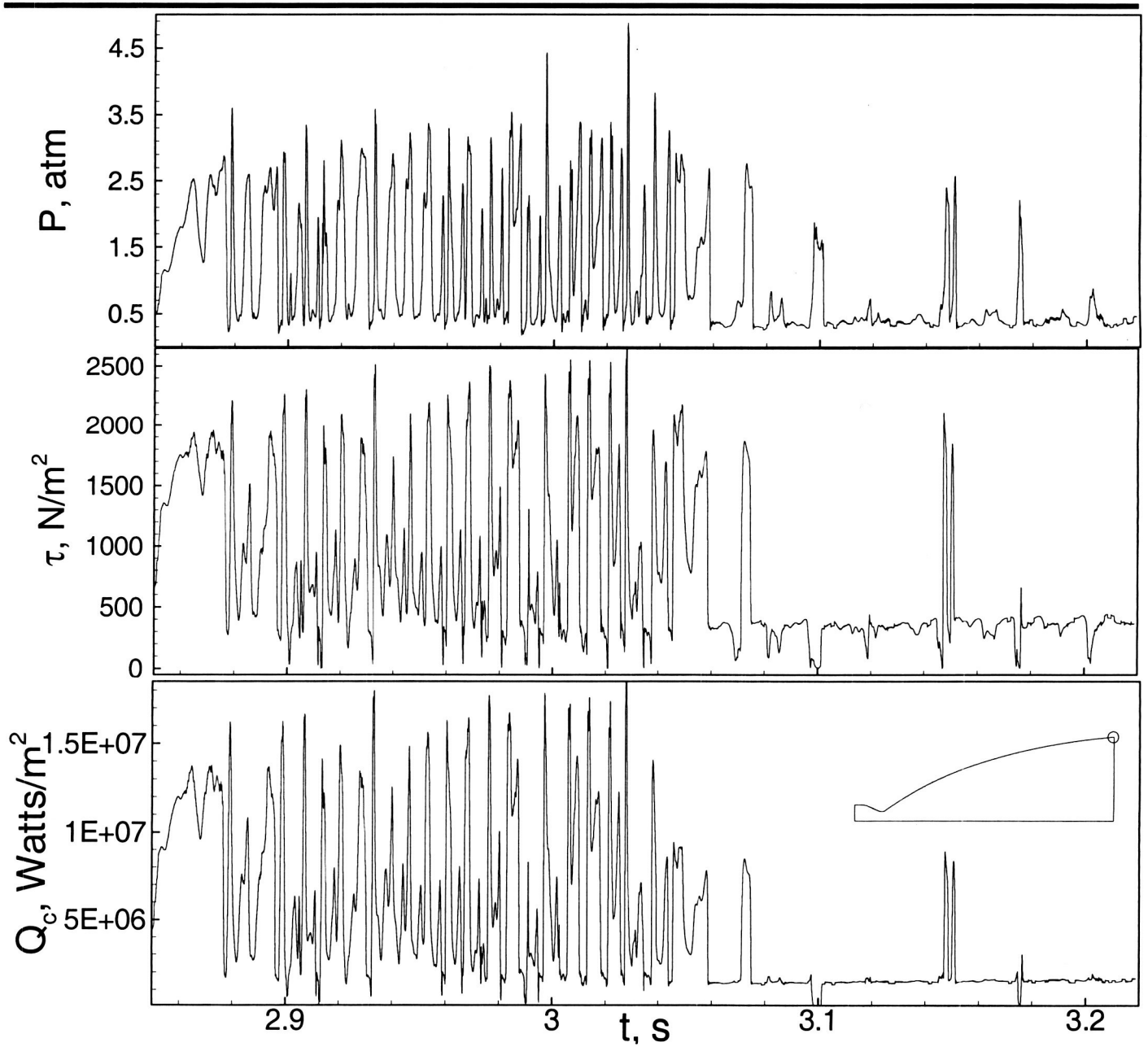

# Computed frequency domain for the cooled nozzle during RSS oscillation across the lip

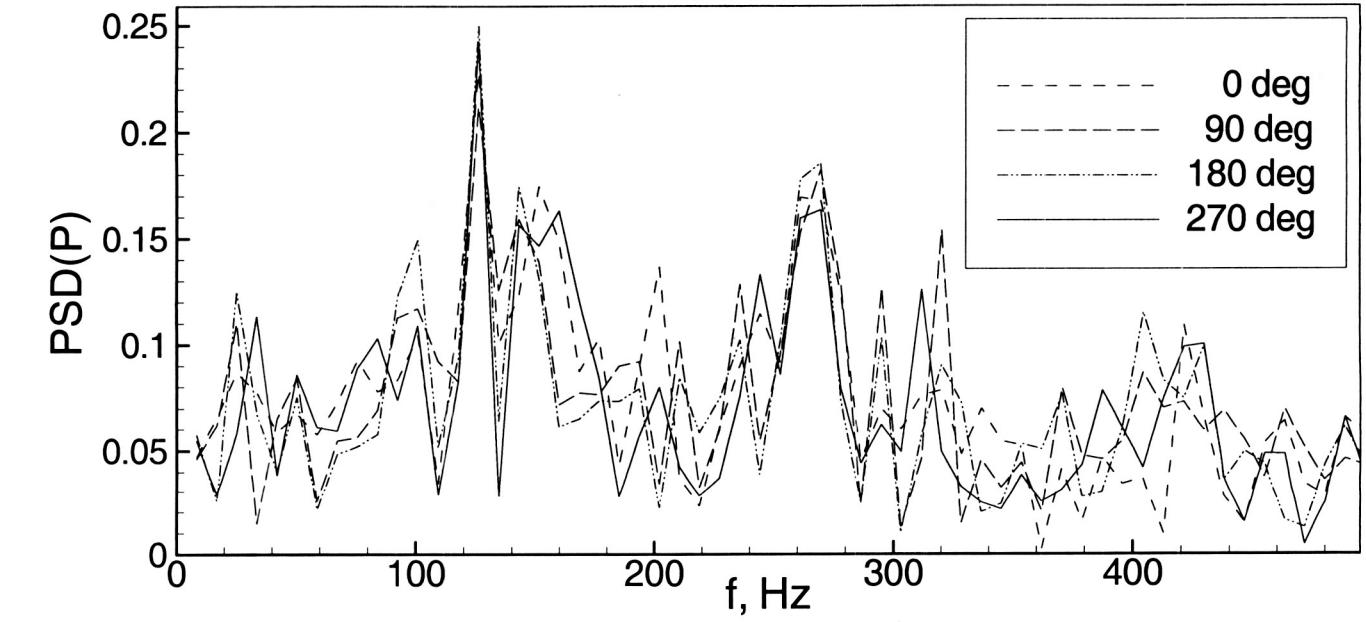


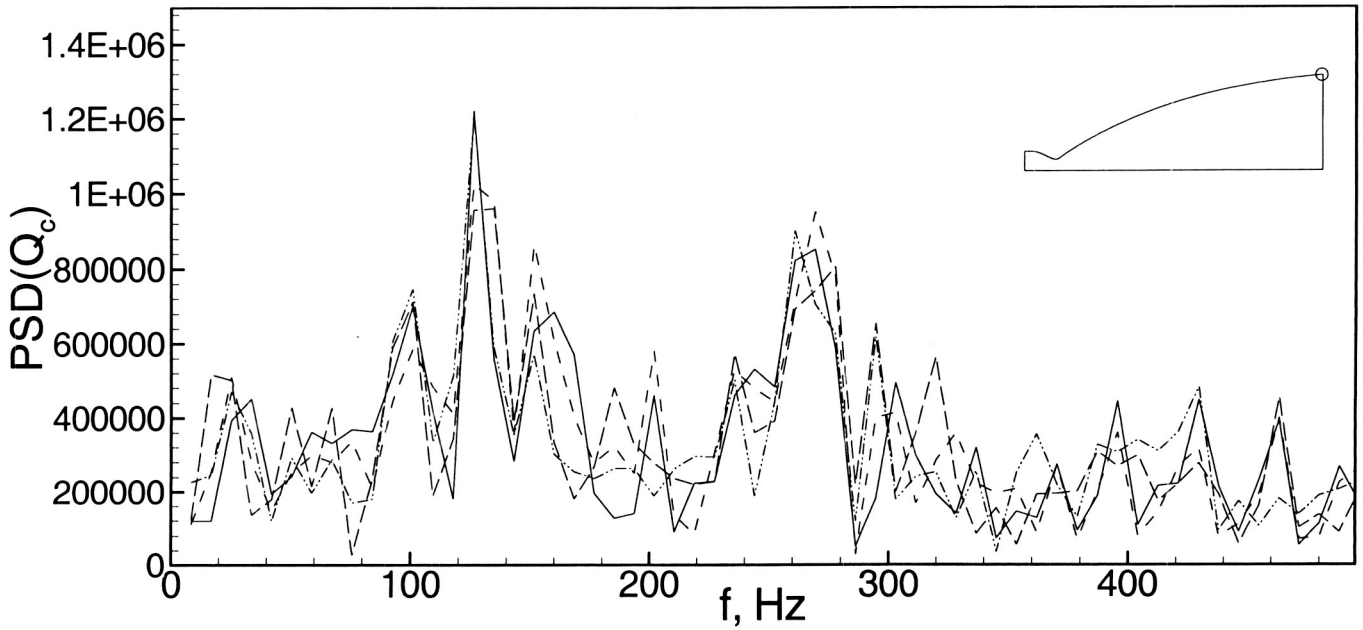

# A comparison of dominant frequencies during shock oscillations across the lip


| | Dominant frequency, Hz | Variable |
|---|---|---|
| Adiabatic nozzle | 45 | pressure |
| | 49 | temperature |
| Cooled nozzle | 122 | pressure |
| | 125 | heat flux |

# A comparison of local peak side loads


| $F_{yz}$, kN | Test | Computation | | |
|---|---|---|---|---|
| | | Adiabatic nozzle | Cooled nozzle | physics |
| - | - | 395 | 176 | Combustion wave |
| 1st mode | 90* | 70 | 80 | FSS-to-RSS transition |
| | | 102 | - | RSS-to-FSS transition |
| 2nd mode | 200* | 110 | - | FSS-to-partial RSS transition |
| | | 60 | - | FSS oscillation across lip |
| | | - | 212 | RSS oscillation across lip |

* Normalized.

# Conclusions


- 3-D numerical studies of the Block-I SSME nozzle start-up side load physics and predictions of the associated aerodynamic side load for adiabatic and cooled nozzles were performed.
- Three types of shock evolutions generate significant side loads: the occurrence of **combustion wave, transitions among FSS, RSS and simultaneous FSS and RSS, and shock oscillations across the lip**.
- Wall boundary conditions affect the computed side load physics.

## Conclusions - continued


- The creation of **combustion wave** and the **FSS-to-RSS transition** are common to both adiabatic and cooled nozzles just after the first pressure rise event. After which the adiabatic nozzle prefers the FSS, while the cooled nozzle favors the RSS.
- After the second pressure event, the peak side load of the **adiabatic nozzle** occurs due to the numerous **transitions between FSS, RSS, and partial RSS**, after which lip FSS oscillations follows until the nozzle flows full; for the **cooled nozzle**, RSS persists throughout, and significant side load happens during the **RSS oscillation across the lip**.
- By comparing the computed results with those of test observations, it is deduced that **cooled wall is a more realistic boundary condition** than that of an adiabatic wall for a regeneratively cooled engine.

## Conclusions - continued


- Since the side load induced by combustion wave may be avoided with sparklers, and that induced by the FSS-to-RSS transition is considerably lower, **the RSS oscillation across the lip along with its associated tangential shock motion** appear to be the dominant side load physics for the regeneratively cooled, high aspect-ratio rocket engines.